clones, BLV-13, bound U5A2-13 mAb but not control rat IgG2a.

2.6. DNA sequencing

Both strands of the BLV-13 cDNA clone with an insert of 2.8 kb were sequenced with synthetic oligonucleotide primers and analyzed with an automated fluorescent DNA sequencer (Applied Biosystems, Foster City, CA). Nucleotides and deduced amino acids were analyzed by comparison with the GenBank database.

2.7. Southern blotting

Plasmid DNA (100 ng) purified from each screened cDNA library was digested with EcoR I/Not I, resolved by electrophoresis and blotted onto nitrocellulose membranes by alkaline transfer. A hybridization probe of 2.8 kb prepared by PCR using 100 pg BLV-13 cDNA as a template was labeled and detected using the commercially available DIG High Prime DNA Labeling and Detection Starter Kit® (Roche; Mannheim, Germany), according to the manufacturer's instructions.

2.8. Western blotting, cell surface biotinylation and immunoprecipitation

The expression of ICAM-1 in COS-7 cells was assessed via immunoblot assay as described [35]. Cell surface proteins of the transfected COS-7 cells were biotinylated using sulfosuccinimidobiotin [36]. After three washes in PBS, cells were suspended at a density of 25×10^6/ml in 0.9% NaCl with 0.01 M HEPES (pH 8.0) and 0.5 mg/ml of Sulfo-NHS-biotin® (Pierce, Rockford, IL) and rocked for 30 min at room temperature. The reaction was terminated by adding 1 M Tris–HCl (pH 7.5) and incubated for an additional 15 min. After centrifugation, cells were disrupted in lysis buffer containing 50 mM Tris–HCl (pH 8.0), 150 mM NaCl and 1% Triton X-100 in the presence of the protease inhibitors aprotinin (2 μg/ml), leupeptin (2 μg/ml) and phenylmethylsulfonyl fluoride (PMSF) (0.57 mM) at 4 °C for 30 min with occasional mixing. After centrifugation, the supernatant served as the cell lysate. The cell lysate was clarified by an incubation with protein G-Sepharose® (Pharmacia, Peapack, NJ), immunoprecipitated with U5A2-13 mAb and anti-ICAM-1 polyclonal Ab for 2 h, then incubated again with protein G-Sepharose for 1 h. After five washes with lysis buffer, protein was eluted directly by boiling for 5 min in SDS sample buffer. The immunoprecipitates were resolved by 7.5% of SDS-PAGE and electrophoretically transferred onto Immobilon® membranes (Millipore, Bedford, MA). Biotinylated protein was detected using avidin and biotinylated horseradish peroxidase macromolecular complex (Vector, Burlingame, CA) and an Enhanced Chemiluminescence (ECL®) kit (Amersham, Aylesbury, UK).

2.9. Cell preparations and flow cytometry

Hepatic mononuclear cells (MNCs) were prepared as described [30]. The liver was removed, pressed through 200 μm gauge stainless steel mesh and suspended in RPMI 1640 containing 5% heat inactivated FCS. After washing with the same medium, the cells were resuspended in 30% Percoll® (Amersham Pharmacia Biotech, Uppsala, Sweden) and 65 U/ml heparin and centrifuged at $750 \times g$ for 15 min at room temperature. The cell pellet was collected and erythrocytes in the hepatic MNC suspension were removed using 0.83% ammonium chloride–Tris buffer. The remaining hepatic MNCs were washed in RPMI 1640 and suspended in SB. Except for when anti-rat IgG-PE was used, the cells were incubated beforehand with Fc-block reagent (2.4G2, anti-CD16/32, BD PharMingen). Hepatic MNCs (1×10^6) were incubated with FITC or PE conjugated mAbs for 30 min at 4 °C, then washed and suspended in SB for analysis using a FACS Calibur® and Cell Quest® software (Becton Dickinson, Mountain View, CA). Except for three-color examinations, cells were gated with propidium iodide (PI). Indirect staining proceeded as described [30].

2.10. Epitope mapping

Peptides were synthesized to include all overlapping linear 30-mers covering the whole mouse ICAM-1 sequence. We also designed peptides in which loops of the five domains were combined in all kinds of orientations, re-creating discontinuous regions of the Ig-like domains. The binding activities of U5A2-13 mAb to these peptides were measured by Pepscan Systems (Lelystad, The Netherlands). Briefly, 2230 overlapping 30-mers, off-set one by one, were synthesized and screened using credit-card format mini-PEPSCAN cards (455 peptide format/card) as described previously [37–39]. The binding of antibody to each peptide was tested in a PEPSCAN-based enzyme-linked immuno assay (ELISA). The 455-well credit-card format polyethylene cards, containing the covalently linked peptides, were incubated with antibody U5A2-13 (10 μg/ml, diluted in blocking solution which contains 5% horse-serum (v/v) and 5% ovalbumin (w/v) and 0.05% Tween 20) (4 °C, overnight). After washing the peptides were incubated with anti-rat IgG horseradish peroxidase (dilution 1/1000 in blocking solution) (1 h, 25 °C), and subsequently, after washing the peroxidase substrate 2,2'-azino-di-3-ethylbenzthiazoline sulfonate (ABTS) and 2 ul/ml 3% H_2O_2 were added. After 1 h the color development was measured. The color development of the ELISA was quantified with a CCD-camera and an image processing system. The setup consists of a CCD-camera and a 55 mm lens (Sony CCD Video Camera XC-77RR, Nikon micro-nikkor 55 mm f/2.8 lens), a camera adaptor (Sony Camera adaptor DC-77RR) and the Image Processing Software package Optimas, version 6.5 (Media Cybernetics,

Silver Spring, MD, USA). Optimas runs on a Pentium II computer system.

The identified reacting peptides were colored in a three-dimensional model of whole mouse ICAM-1, 1ic1.pdb, which was derived from the PDB-database [40] and was visualized using the software package Swiss PDB-viewer 3.7b1.

3. Results

3.1. Molecular cloning of a full-length cDNA encoding the antigen recognized by U5A2-13 mAb

We applied an expressional cloning strategy using COS-7 cells to isolate the gene encoding the antigen recognized
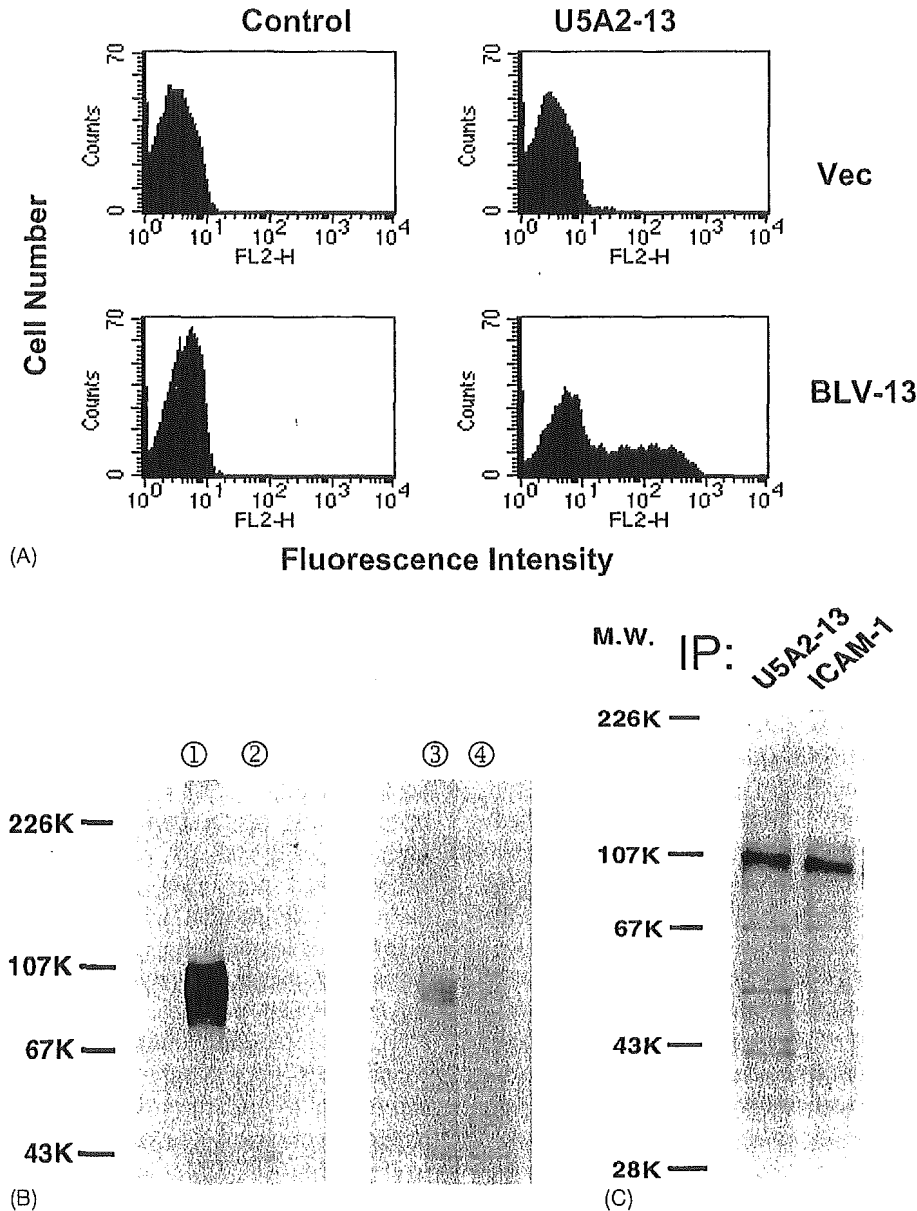

Fig. 1. Surface expression and biochemical analysis of U5A2-13-reactive molecules in COS-7 cells transfected with clone BLV-13 cDNA. (A) U5A2-13 mAb binds to COS-7 cells transfected with clone BLV-13 cDNA. COS-7 cells were transfected with pME18S vector alone (Vec) or with clone BLV-13 cDNA in pME18S (BLV-13), as indicated, right. Transfectants were stained with either PE-conjugated U5A2-13 mAb (U5A2-13) or PE-conjugated isotype-matched control Ab (Control) as indicated, above panel. Ab binding was detected by flow cytometry. (B) Western blotting of COS-7 cells transfected with clone BLV-13. Whole lysates of COS-7 cells transfected with clone BLV-13 were Western blotted. Lanes 1 and 2, transfected and control COS-7 cells detected with anti-ICAM-1 Ab, respectively; lanes 3 and 4, transfected and control COS-7 cells stained with anti-ICAM-1 Ab plus its blocking peptides, respectively. (C) Immunoprecipitation analysis of protein encoded by clone BLV-13 cDNA. Cells were labeled with biotin, then proteins were immunoprecipitated with U5A2-13 mAb and anti-ICAM-1 Ab. Immunoprecipitates were denatured with SDS sample buffer containing 2-ME and resolved in 7.5% SDS-PAGE gels and blotted. The blot was visualized using avidin-biotinylated horseradish peroxidase macromolecular complex and ECL® detection reagents.

by U5A2-13 mAb. A cDNA library was generated from murine BCL1 cells that were positive for U5A2-13 mAb using a pME18S expression vector. Not only NKT cells, but also some murine leukemia cell lines including BCL1, react with U5A2-13 mAb, but BCL1 expresses the most antigen (data not shown). A transfectant of a 2.8 kb cDNA clone, termed BLV-13, that was selected after two cycles of enrichment bound U5A2-13 mAb but not isotype-matched control IgG (Fig. 1A). Before sequencing this cDNA clone, we confirmed its enrichment in the second-round cDNA library by Southern blotting. Sequence analysis demonstrated that BLV-13 cDNA consisted of 2574 bp, encoding a polypeptide with 537 amino acid residues. A GenBank search revealed that the deduced amino acid sequence of BLV-13 was identical to mouse ICAM-1 (GenBank accession no. P13597).

We then Western blotted and immunoprecipitated lysates from BLV-13-transfected COS-7 cells using U5A2-13 and anti-ICAM-1 Abs. A band stained by anti-ICAM-1 Ab in the lysates of BLV-13-transfected COS-7 cells was dimin-

ished by its blocking peptides (Fig. 1B). Immunoprecipitates obtained from BLV-13-transfected COS-7 cells using U5A2-13 and anti-ICAM-1 Abs were detected as a 100 kDa protein band that corresponded to the molecular mass of mouse ICAM-1 (Fig. 1C). To confirm that U5A2-13 mAb reacts with mouse ICAM-1, hepatic mononuclear cells isolated from C57BL/6 mice and ICAM-1 deficient mice were dual-stained with anti-CD3 and one of U5A2-13, anti-ICAM-1 (clone 3E2) or anti-NK1.1 mAbs. We examined two strains of ICAM-1 mutant (exons 4 and 5) mice. U5A2-13 mAb was negative in both strains of ICAM-1 gene targeted mice (Fig. 2). These data demonstrated that our U5A2-13 mAb recognizes ICAM-1.

Furthermore, we sequenced 500 clones obtained from the cDNA library constructed after two cycles of enrichment (data not shown). One-hundred-and-twenty-three out of 500 clones had precisely the same cDNA insert as the 2.8 kb BLV-13 clone, suggesting the absence of an alternative splicing variant other than ICAM-1 mRNA encoding a specific protein recognized by U5A2-13 mAb. No other
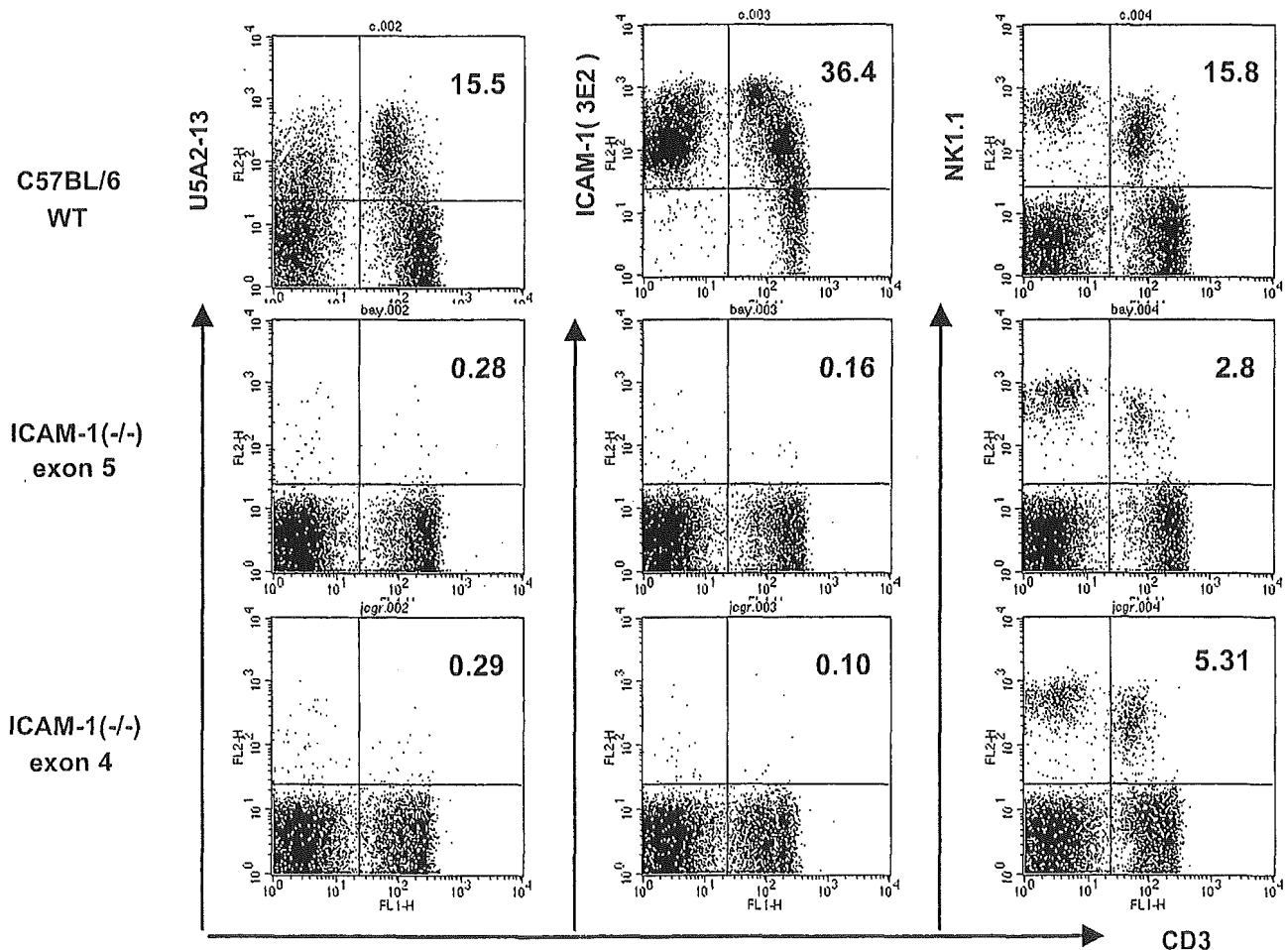

Fig. 2. U5A2-13 mAb did not react with lymphocytes in ICAM-1 deficient mice. Fresh hepatic mononuclear cells were isolated from C57BL/6 and two strains of mice deficient in ICAM-1 (exon 4 mutant and exon 5 mutant) then dual-stained with anti-CD3 mAb and one of U5A2-13 mAb, anti-ICAM-1 (clone 3E2) mAb, or anti-NK1.1 mAb. Data are representative of five individual experiments with similar results.
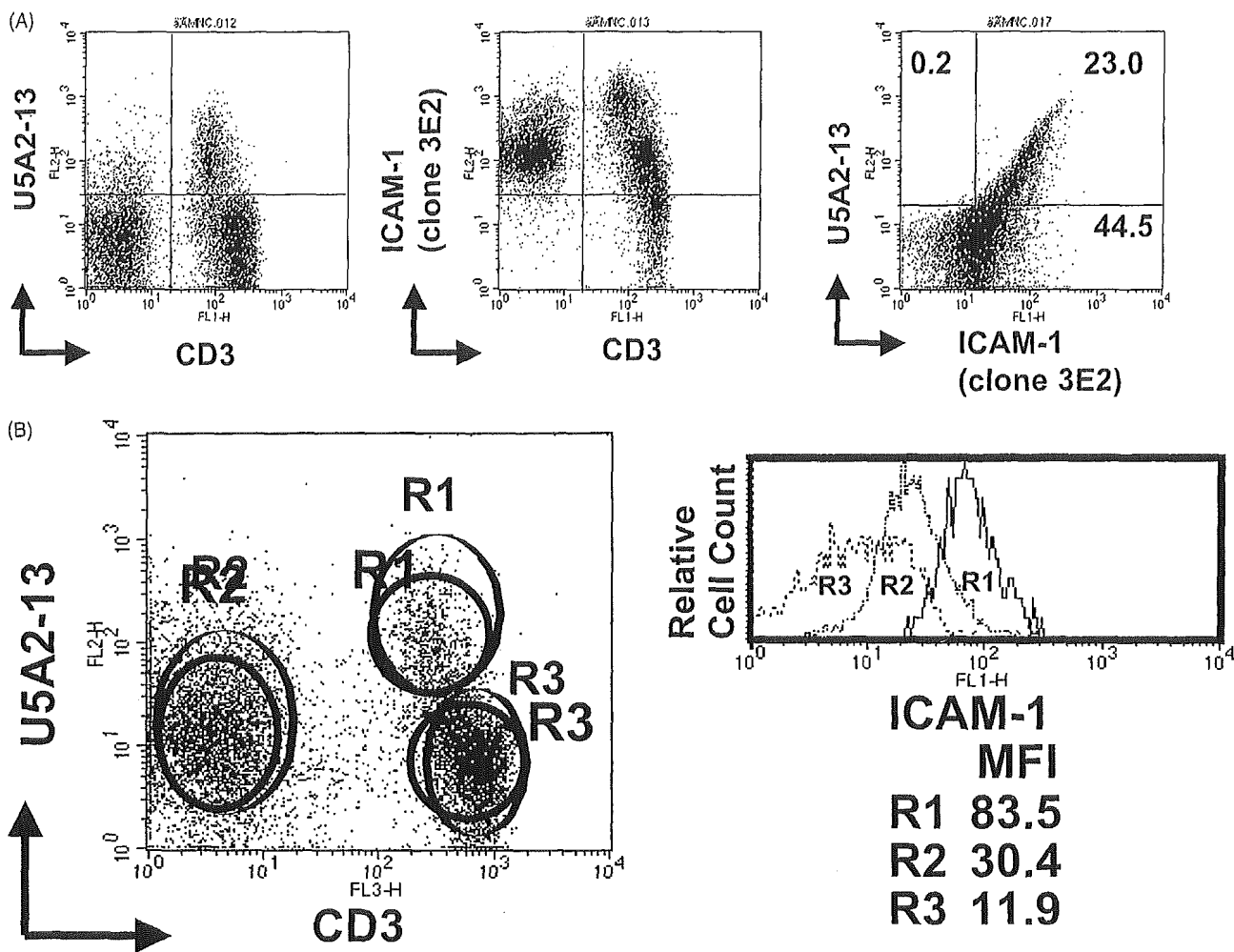
Fig. 3. Flow cytometry revealed that U5A2-13+ T cells correspond to ICAM-1^{high} T cells. Fresh hepatic mononuclear cells were isolated from C57BL/6 and stained with anti-CD3 mAb, U5A2-13 mAb and anti-ICAM-1 (clone 3E2) mAb (A). Mean fluorescence intensity (MFI) of ICAM-1 for each gated region is indicated below the panel (B). Data are representative of three individual experiments with similar results.

genes encoding a cell surface protein were found among the remaining 377 clones.

3.2. NKT cells express an epitope recognized by U5A2-13 mAb in extracellular domain two of ICAM-1

The profiles of hepatic mononuclear cells dual-stained with anti-CD3 mAb and one of U5A2-13, or anti-ICAM-1 (clone 3E2) mAbs were quite different (Fig. 3A). Three-color flow cytometry demonstrated that the U5A2-13 positive population encompasses CD3 positive, ICAM-1 (3E2) bright subsets, corresponding to approximately 35% of the 3E2 positive population (Fig. 3B). Flow cytometry revealed that the mean florescence intensity of ICAM-1 is very high not only murine, but also in human TCR Vα24 positive NKT cells (unpublished data).

We examined whether or not the epitopes of the antibodies are different, by performing a competitive inhibition assay. U5A2-13 mAb staining was not blocked by a prior incubation with other anti-ICAM-1 mAbs such as clone 3E2, KAT-1, or YN1/1 (data not shown).

In addition, in order to determine U5A2-13 epitope, we generated synthetic peptides that represent amino acid sequences of ICAM-1 and examined their reactivity with U5A2-13 mAb by ELISA. Synthetic rod-attached peptides were used to map the antigenic sites on the extracellular domain of the ICAM-1. By means of the Pepscan method, all possible 2230 overlapping 30-mer peptides, composed of two 15-mer parts derived from the primary sequence, were synthesized. U5A2-13 mAb was tested against the synthetic minicard-peptides. Peptides were considered to represent antigenic sites if peaks occurred in a set of neighboring peptides and if at least one of the peaks in such a set amounted to more than three times the background. U5A2-13 mAb recognized a discontinuous epitope that was made of three parts of extracellular domain two of ICAM-1. The identified sites are: 161–178 region in B–C loop, 135–151 region in C′–E loop, and 188–204 region in F–G loop (Fig. 4).

Domain 1

Domain 2

SAVLLRGEELSRQPVGGHPKDPKEIFFTVLASRGD   B-C
HVDGGAPRTQLSAVLLR   C'-E
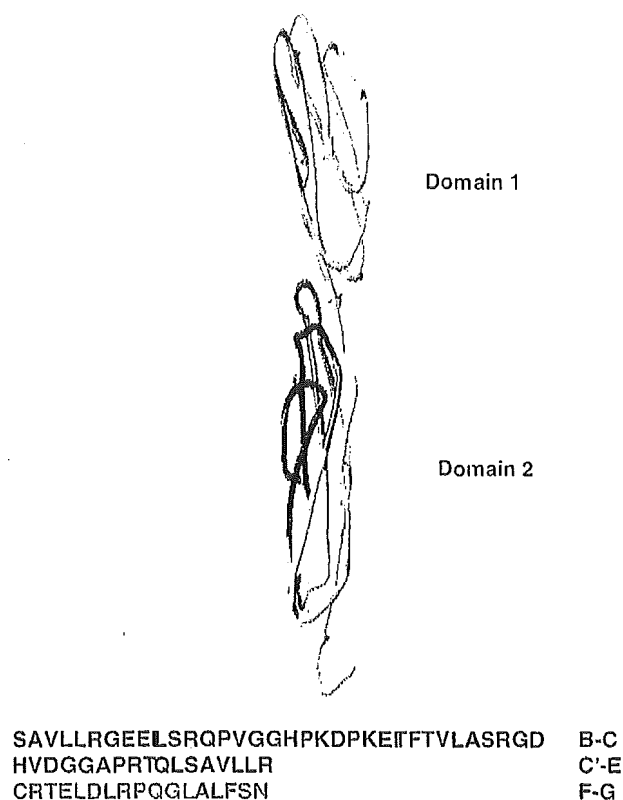CRTELDLRPQGLALFSN   F-G

Fig. 4. U5A2-13 epitope in a 3D model of human ICAM-1. U5A2-13 epitope consists of three loops in domain two of ICAM-1. The three homologous regions are demonstrated in a model of human ICAM-1(GenBank accession no. MMDB 8008). The core epitope is depicted in red. Two adjacent loops in blue and green are also part of the epitope.

Collectively, these data suggest that NKT cells express a unique epitope of ICAM-1 recognized by U5A2-13 mAb.

4. Discussion

Our studies demonstrated that an NKT cell surface antigen recognized by a novel mAb, U5A2-13, is encoded by *ICAM-1* gene and that its discontinuous epitope is composed of three loops located in extracellular domain two of ICAM-1. Expression of the classical NK marker, NK1.1 antigen, is confined to C57BL/6 and related strains, which hampers investigation in disease models of NK1.1-negative strains [1,2]. We showed previously that U5A2-13^{+} T cells encompass a population functionally similar to NK1.1^{+} T cells in various mouse strains such as C57BL/6, BALB/c, and C3H/He [28,30,31]. Furthermore, staining with U5A2-13 mAb yielded higher signal intensity for NKT cells than NK cells in FACS® analyses. This is unique compared with antibodies of other NK markers such as NK1.1, IL-2Rβ, Ly49 or DX5.

Recently the antigen recognized by DX5 has been molecularly cloned, which revealed CD49b (Very Late Antigen-2) [41]. Like U5A2-13, a surrogate NK marker, DX5, also corresponds to an adhesion molecule. This is not fortuitous but rather suggests that the importance of adhesion molecules

cannot be over-emphasized in NK and NKT cell function. NKT cells are considered to activate NK cells rapidly in the innate immune system [9]. NK cells express large amount of LFA-1 [42]. Our study showed that NKT cells express ICAM-1 most. This constitutes a reasonable evidence for efficient cross-talk between these cells.

The staining profiles of hepatic MNCs with U5A2-13 mAb and with other conventional anti-ICAM-1 mAbs (such as 3E2, YN1/1 or KAT-1) were quite different (Fig. 3A). U5A2-13 epitope resides in domain two. The epitopes of the other anti-ICAM-1 antibodies, on the other hand, are located in domain one, which is the site responsible for binding with its ligand LFA-1. Therefore, in competitive inhibition assay, staining with U5A2-13 mAb was not blocked by these antibodies (unpublished observation). We cannot exclude a possibility that, because of its affinity for ICAM-1, U5A2-13 mAb recognizes only the ICAM-1^{high} population when ICAM-1 is present in substantial amounts on the cell surface. Another possibility is that freshly isolated naïve NKT cells express a unique epitope in domain two of ICAM-1 in such a manner that it can efficiently react with U5A2-13 mAb. The ICAM-1 epitope recognized by U5A2-13 mAb may depend on glycosylation selective to NK cells. Accumulating evidence shows that ICAM-1 forms homodimers on the cell surface that are more efficient than monomers in binding to its ligand, LFA-1 [43–46]. In freshly harvested mononuclear cells, staining with U5A2-13 mAb is mostly confined to NKT cells but not to conventional T and B cells. We also revealed that, upon activation by a mitogen, not only NKT cells but also T and B cells start to react with U5A2-13 mAb [47]. Taken together, these findings may indicate that homodimers of ICAM-1 on the surface of activated ICAM-1^{high} cells form an epitope for U5A2-13 mAb. ICAM-1 per se is widely expressed on lymphocytes but it is not until they get fully activated and become ICAM-1^{high} when they begin to show U5A2-13 epitope otherwise concealed. Similarly, NK1.1 antigen is also induced on CD8^{+} T cells upon activation [48].

It is of interest that this U5A2-13 epitope on NKT cells is related to their recognition and functions. In vivo administration of U5A2-13 mAb not only modulates cytokines production by NKT cells upon stimulation with α-GalCer but also increases tumor metastases in a B16 melanoma model (manuscript in preparation). We conclude that NKT cells express a unique U5A2-13 epitope of ICAM-1.

Acknowledgements

References

[1] Bendelac A, Rivera MN, Park SH, Roark JH. Mouse CD1-specific NK1 T cells: development, specificity, and function. Annu Rev Immunol 1997;15:535–62.

[2] Godfrey DI, Hammond KJL, Poulton LD, Smyth MJ, Baxter AG. NKT cells: facts, functions and fallacies. Immunol Today 2000;21:573–83.

[3] Bix M, Locksley RM. Natural T cells. Cells that co-express NKRP-1 and TCR. J Immunol 1995;155:1020–2.

[4] MacDonald HR. NK1$^+$ T cell receptor-α/β^+ cells: new clues to their origin, specificity, and function. J Exp Med 1995;182:633–8.

[5] Fowlkes BJ, Kruisbeek AM, Ton-That H, Weston MA, Coligan JE, Schwartz RH, et al. A novel population of T-cell receptor α, β-bearing thymocytes which predominantly expresses a single V_β gene family. Nature 1887;329:251–4.

[6] Makino Y, Kanno R, Ito T, Higashino K, Taniguchi M. Predominant expression of invariant $V_\alpha 14^+$ TCR α chain in NK1.1$^+$ T cell populations. Int Immunol 1995;7:1157–61.

[7] Hong S, Scherer DC, Singh N, Mendiratta SK, Serizawa I, Koezuka Y, et al. Lipid antigen presentation in the immune system: lessons learned from CD1d knockout mice. Immunol Rev 1999;169:31–44.

[8] Nakagawa R, Motoki K, Ueno H, Iijima R, Nakamura H, Kobayashi E, et al. Treatment of hepatic metastasis of the colon adenocarcinoma with an α-galactosylceramide, KRN7000. Cancer Res 1998;58:1202–7.

[9] Carnaud C, Lee D, Donnars O, Park SH, Beavis A, Koezuka Y, et al. Cross-talk between cells of the innate immune system: NKT cells rapidly activate NK cells. J Immunol 1999;163:4647–50.

[10] Takahashi T, Nieda M, Koezuka Y, Nicol A, Porcelli SA, Ishikawa Y, et al. Analysis of human Vα 24$^+$CD4$^+$ NKT cells activated by α-glycosylceramide-pulsed monocyte-derived dendritic cells. J Immunol 2000;164:4458–64.

[11] Yoshimoto T, Bendelac A, Watson C, Hu-Li J, Paul WE. Role of NK1.1$^+$ T cells in a T_H2 response and in immunoglobulin E production. Science 1995;270:1845–7.

[12] Kawano T, Cui J, Koezuka Y, Toura I, Kaneko Y, Motoki K, et al. CD1d-restricted and TCR-mediated activation of Vα14 NKT cells by glycosylceramides. Science 1997;278:1626–9.

[13] Burdin N, Brossay L, Koezuka Y, Smiley ST, Grusby MJ, Gui M, et al. Selective ability of mouse CD1d to present glycolipids: α-galactosylceramide specifically stimulates Vα 14$^+$ lymphocytes. J Immunol 1998;161:3271–81.

[14] Brossay L, Chioda M, Burdin N, Koezuka Y, Casorati G, Dellabona P, et al. CD1d-mediated recognition of an α-galactosylceramide by natural killer T cells is highly conserved through mammalian evolution. J Exp Med 1998;188:1521–8.

[15] Spada FM, Koezuka Y, Porcelli SA. CD1d-restricted recognition of synthetic glycolipid antigens by human natural killer T cells. J Exp Med 1998;188:1529–34.

[16] Hammaond KJL, Pellicci DG, Poulton LD, Naidenko OV, Scalzo AA, Baxter AG, et al. CD1d-restricted NKT cells: an interstrain comparison. J Immunol 2001;167:1164–73.

[17] Metelitsa LS, Naidenko OV, Kant A, Wu HW, Loza MJ, Perussia B, et al. Human NKT cells mediate antitumor cytotoxicity directly by recognizing target cell CD1d with bound ligand or indirectly by producing IL-2 activate NK cells. J Immunol 2001;167:3114–22.

[18] Chen H, Huang H, Paul WE. NK1.1$^+$CD4$^+$ T cells lose NK1.1 expression upon in vitro activation. J Immunol 1997;158:5112–9.

[19] Ito T, Ishibashi K, Imai K, Koseki H, Ra C, Fernandez E, et al. Monoclonal antibody against murine T cell receptor Vα14 cross-reacts with human CD3 ε and detects disulfide-linked dimeric form. Int Immunol 1991;3:991–5.

[20] Benlagha K, Weiss A, Beavis A, Teyton L, Bendelac A. In vivo identification of glycolipid antigen-specific T cells using CD1d tetramers. J Exp Med 2000;191:1895–903.

[21] Matsuda JL, Naidenko OV, Gapin L, Nakayama T, Taniguchi M, Wang CR, et al. Tracking the response of natural killer T cells to a glycolipid antigen using CD1d tetramers. J Exp Med 2000;192:741–53.

[22] Eberl G, Lees R, Smiley ST, Taniguchi M, Grusby MJ. MacDonald HR. Tissue-specific segregation of CD1d-dependent and CD1d-independent NKT cells. J Immunol 1999;162:6410–9.

[23] Zeng D, Gazit G, Dejbakhsh-Jones S, Balk SP, Snapper S, Taniguchi M, et al. Heterogeneity of NK1.1$^+$ T cells in the bone marrow: divergence from the thymus. J Immunol 1999;163:5338–45.

[24] Hammond KJL, Pelikan SB, Crowe NY, Randle-Barrett E, Nakayama T, Taniguchi M, et al. NKT cells are phenotypically and functionally diverse. Eur J Immunol 1999;29:3768–81.

[25] MacDonald HR. CD1d-glycolipid tetramers: a new tool to monitor natural killer T cells in health and disease. J Exp Med 2000;192:F15–9.

[26] Dang Y, Heyborne KD. Regulation of uterine NKT cells by a fetal Class I molecule other than CD1d. J Immunol 2001;166:3641–4.

[27] Hameg A, Apostolou I, Leite-de-Moraes M, Gombert JM, Garcia C, Koezuka Y, et al. A subset of NKT cells that lacks the NK1.1 marker, expresses CD1d molecules, and autopresents the α-galactosylceramide antigen. J Immunol 2000;165:4917–26.

[28] Maruoka H, Ikarashi Y, Shinohara K, Miyata M, Sugimura T, Terada M, et al. A novel monoclonal antibody permitting recognition of NKT cells in various mouse strains. Biochem Biophys Res Commun 1998;242:413–8.

[29] Wakasugi H, Koyama K, Gyotoku M, Yoshimoto M, Hirohashi S, Sugimura T, et al. Frequent development of murine T-cell lymphomas with TcR α/β^+, CD4$^-$/8$^-$ phenotype after implantation of human inflammatory breast cancer cells in BALB/c nude mice. Jpn J Cancer Res 1995;86:1086–96.

[30] Shinohara K, Ikarashi Y, Maruoka H, Miyata M, Sugimura T, Terada M, et al. Functional and phenotypical characteristics of hepatic NK-like T cells in NK1.1-positive and -negative mouse strains. Eur J Immunol 1999;29:1871–8.

[31] Azuma M, Kato K, Ikarashi Y, Asada-Mikami R, Maruoka H, Takaue Y, et al. Cytokines production of U5A2-13-positive T cells by stimulation with glycolipid α-galactosylceramide. Eur J Immunol 2000;30:2138–46.

[32] Seed B, Aruffo A. Molecular cloning of the CD2 antigen, the T-cell erythrocyte receptor, by a rapid immunoselection procedure. Proc Natl Acad Sci USA 1987;84:3365–9.

[33] Hayashida K, Kitamura T, Gorman DM, Arai K, Yokota T, Miyajima A. Molecular cloning of a second subunit of the receptor for human granulocyte-macrophage colony-stimulating factor (GM-CSF): reconstitution of a high-affinity GM-CSF receptor. Proc Natl Acad Sci USA 1990;87:9655–8.

[34] Yamasaki K, Taga T, Hirata Y, Yawata H, Kawanishi Y, Seed B, et al. Cloning and expression of the human interleukin-6 (BSF-2/IFNβ2) receptor. Science 1988;241:825–8.

[35] Yoshida M, Feng W, Nishio K, Takahashi M, Heike Y, Saijo N, et al. Antitumor action of the PKC activator gnidimacrin through CDK2 inhibition. Int J Cancer 2001;94:348–52.

[36] Altin JG, Pagler EB. A one-step procedure or biotinylation and chemical cross-linking of lymphocyte surface and intracellular membrane-associated molecules. Anal Biochem 1995;224:382–9.

[37] Slootstra JW, Puijk WC, Ligtvoet GJ, Langeveld JP, Meloen RH. Structural aspects of antibody–antigen interaction revealed through small random peptide libraries. Mol-Divers 1996;1:87–96.

[38] Slootstra JW, Puijk WC, Meloen RH, Schaaper WMM. Mapping of discontinuous epitopes on FSH. In: Proceedings of the Second International and the 17th American Peptide Symposium on Peptides, the Wave of the Future, 2001. p. 189–90.

[39] Schaaper WMM, Slootstra JW, Puijk WC, van Dijik E, Porter P, Davis PJ, et al. Matrix-scan as effective tool to map discontinuous epitopes. In: Proceedings of the 27th European Peptide Symposium on Peptides 2002, 2002. p. 1008–9.

[40] Berman HM, Westbrook J, Feng Z, Gilliland G, Bhat TN, Weissig H, et al. The protein data bank. Nucl Acids Res 2000;28:235–42.

[41] Arase H, Saito T, Phillips JH, Lalnier LL. The mouse NK cell-associated antigen recognized by DX5 monoclonal antibody is CD49b (α_2 integrin, Very Late Antigen-2). J Immunol 2001;167:1141–4.

[42] Matsumoto G, Omi Y, Lee U, Nishimura T, Shindo J, Penninger JM. Adhesion mediated by LFA-1 is required for efficient IL-12-induced NK and NKT cell cytotoxicity. Eur J Immunol 2000;30:3723–31.

[43] Reilly PL, Woska Jr JR, Jeanfavre DD, McNally E, Rothlein R, Bormann BJ. The native structure of intercellular adhesion molecule-1 (ICAM-1) is a dimmer. J Immunol 1995;155:529–32.

[44] Miller J, Knorr R, Ferrone M, Houdei R, Carron CP, Dustin ML. Intercellular adhesion molecule-1 dimerization and its consequences for adhesion mediated by lymphocyte function associated-1. J Exp Med 1995;182:1231–41.

[45] Casasnovas JM, Stehle T, Liu JH, Wang JH, Springer TA. A dimeric crystal structure for the N-terminal two domains of intercellular adhesion molecule-1. Proc Natl Acad Sci USA 1998;95:4134–9.

[46] Jun CD, Shimaoka M, Carman CV, Takagi J, Springer TA. Dimerization and the effectiveness of ICAM-1 in mediating LFA-1-dependent adhesion. Proc Natl Acad Sci USA 2001;98:6830–5.

[47] Kato K, Ikarashi Y, Sugahara T, Yasumoto A, Sancho D, Yoshida M, et al. U5A2-13, an antigen originally found on mouse NK-like T cells, is an early inducible cell surface antigen during lymphoid activation. Cell Immunol 2003;221:27–36.

[48] Assarsson E, Kambayashi T, Sandberg JK, Hong S, Taniguchi M, Van Kaer L, et al. CD8+ T cells rapidly acquire NK1.1 and NK cell-associated molecules upon stimulation in vitro and in vivo. J Immunol 2000;165:3673–9.

ROLE OF NATURAL KILLER T CELLS IN ANTI-TUMOR IMMUNE RESPONSE

Yoshinori Ikarashi, Yuji Heike, Atsushi Shimizu, Osamu Imataki
Sachiyo Kanai, Mitsuzi Yoshida, Akira Iiduka, Takayuki Morikawa
Yoichi Takaue[1], and Hiro Wakasugi
Pharmacology Division, Hematopoietic Stem Cell Transplantation/Immunotherapy Unit[1]
National Cancer Center Research Institute
5-1-1 Tsukiji, Chuo-ku, Tokyo 104-0045, Japan
(hwakasug@gan2.ncc.go.jp)

1. Introduction

Natural killer T (NKT) cells are reportedly involved in tumor rejection. NKT cells in mice are usually defined as lymphocytes expressing intermediate levels of TCR and NK cell-associated molecules, particularly NK1.1. They predominantly express TCR with invariant $V\alpha14J\alpha281/V\beta8$, 7, or 2 in mice or $V\alpha24J\alpha Q/V\beta11$ in humans, and most are phenotypically double-negative ($CD4^-CD8^-$) or single-positive ($CD4^+CD8^-$) T cells. These cells produce large amounts of interferon (IFN)-γ and interleukin (IL)-4, suggesting that they play an important role in regulating Th1/Th2 balance, including tumor immunity. Most NKT cells are restricted by CD1d molecule and react strongly to sponge-derived glycolipid α-galactosylceramide (α-GalCer)[1].

2.NKT cells express a unique epitope of ICAM-1 that plays a role in tumor rejection

2.1 Establishment of monoclonal antibody U5A2-13: NKT cells in mice are generally defined as NK1.1$^+$ T cells, although NK1.1 antigen is expressed only in C57BL/6 and related strains. This has precluded investigations of other strains. To identify a novel NKT cell-surface marker irrespective of strain, we generated the monoclonal antibody (mAb) U5A2-13[2], which phenotypically and functionally identifies populations that are similar to NKT cells. This mAb was originally obtained by immunizing a Fischer rat with tMK-2U lymphoma cells from a BALB/c nude mouse carrying xenografted human inflammatory breast tumor cells.

We have shown that U5A2-13$^+$ T cells predominantly use TCR Vβ8, 7 or 2, and that,

similar to NK1.1^{+} T cells, U5A2-13^{+} T cells can produce both IFN-γ and IL-4 upon cross linking with CD3[3]. We have also demonstrated that hepatic U5A2-13^{+} T cells recognize the NKT cell ligand, α-GalCer, as presented by CD1d molecules on dendritic cells[4]. These results indicate that U5A2-13 mAb represents a valuable tool for studying NKT cells in NK1.1-negative mouse strains. However, flow cytometry revealed that the cell surface molecule recognized by U5A2-13 mAb differs from other NK lineage molecules such as NK1.1, Ly-49, 2B4 and DX5[5]. To elucidate the U5A2-13 antigen on NKT cells, the antigen was cloned using expressional cloning. The amino acid sequence of BLV-13 clone was identical to mouse ICAM-1. To confirm that U5A2 reacts with ICAM-1, hepatic mono- nuclear cells from B6 and ICAM-1 mutant mice were stained. U5A2 was negative in two available strains of ICAM-1 K/O mice. These data demonstrated that our U5A2 recog- nizes really ICAM-1. Note that the staining pattern of U5A2-13 mAb differs considerably from that of ICAM-1. U5A2-13 mAb was found to recognize ICAM-1 high-expressing cell population and this population is around 30% of ICAM-1-positive T cells. Our results seem to indicate that U5A2-13 mAb recognizes a unique epitope expressed only in NKT cells. We therefore performed epitope mapping and revealed that the U5A2 epitope com- prises three loops of the extracellular domain 2 of ICAM-1, whereas all available Abs recognize epitopes of domain 1. Prior studies have shown that the number of NKT cells is decreased in LFA-1 K/O mice. In our study, the number of NKT cells was found to be further decreased in ICAM-1-deficient mice. This suggests that ICAM-1/LFA-1 interac- tions and associated signaling pathways are important in the differentiation of NKT cells.
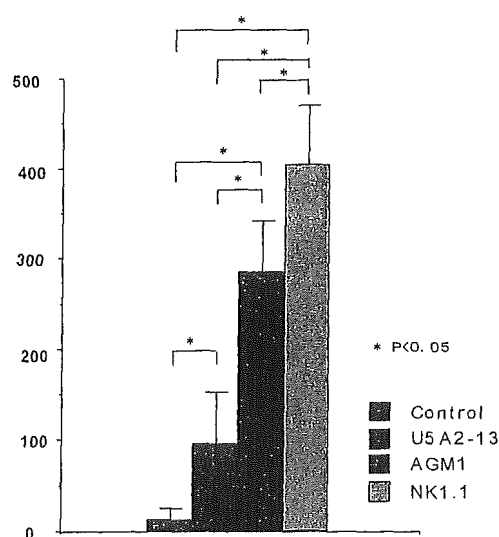

Fig.1 B16 Melanoma Lung Metastases after Ab Treatment

2.2 A unique epitope of ICAM-1 that plays a role in tumor rejection: Here, we investigated whether the U5A2-13 epitope on NKT cells is responsible for anti-tumor activities. To assess the contribution of NKT cells compared with NK cells in a lung metastasis model, mice were treated with U5A2-13 mAb, anti-asialo GM1 (AGM1) Ab, and anti-NK1.1 mAb, then inoculated with B16 melanoma cells. In contrast with anti-NK1.1 antibody, *in vivo* treatment with U5A2-13 did not reduce the number of NKT cells, but resulted in shedding of ICAM-1 from the NKT cell surface, thus increasing serum levels of soluble ICAM-1. U5A2-13 mAb *in vivo* down-regulated U5A2-13 epitope expression, whereas numbers of NK1.1$^+$ T cells remained stable. Anti-AGM1 Ab *in vivo* depleted NK cells, whereas numbers of NK1.1$^+$ and U5A2-13$^+$ T cells remained stable. Anti-NK1.1 mAb *in vivo* depleted NK, NK1.1$^+$ T and U5A2-13$^+$ T cells. Tumor growth-promoting effects were augmented by, in ascending order, U5A2-13 mAb, anti-AGM1 Ab, and anti-NK1.1 mAb (Fig.1). Collectively, these data suggest that the presence of U5A2-13 epitope is important for NKT cells to control tumor metastasis in the B16 melanoma model.

3. Expansion of Th0-type NK1.1⁻ CD1d-restricted NKT cells by α-GalCer stimulation

3.1 Expansion of three distinct NKT cell populations by IL-2 and α-GalCer: To characterize α-GalCer–activated NKT cells *in vitro*, murine splenic mononuclear cells (MNCs) were cultured with or without 50 ng/ml of α-GalCer and 100 U/ml of human IL-2. Before culturing, a small percentage of NK1.1$^+$ T cells ($1.01\pm0.24\%$) and CD1d/α-GalCer tetramer$^+$ T cells ($1.01\pm0.18\%$) were identified in splenic MNCs. Percentages of NK1.1$^+$CD1d/α-GalCer tetramer$^+$ cells and NK1.1⁻CD1d/α-GalCer tetramer$^+$ cells in T cells were $0.95\pm0.52\%$ and $0.88\pm0.54\%$, respectively. On day 6, percentages of NK1.1$^+$ T cells and NK cells were increased when cultured with IL-2 and α-GalCer or IL-2 alone. However, the percentage of CD1d/α-GalCer tetramer$^+$ T cells was increased in culture with IL-2 and α-GalCer, but not in culture with IL-2 alone. These results indicate that IL-2 induces expansion of NK1.1$^+$ T cells, whereas α-GalCer induces expansion of CD1d/α-GalCer tetramer$^+$ T cells that are able to react to α-GalCer.

Next, we examined whether CD1d/α-GalCer tetramer$^+$ NKT cells express NK1.1 molecules. Almost none of the CD1d/α-GalCer tetramer$^+$ NKT cells expanded with IL-2 and α-GalCer expressed NK1.1 molecules. This indicates that three distinct murine NKT-cell subsets are expanded after IL-2 and α-GalCer activation *in vitro*: NK1.1⁻CD1d/α-GalCer tetramer$^+$ NKT cells; NK1.1$^+$CD1d/α-GalCer tetramer$^+$ NKT cells; and NK1.1$^+$CD1d/α-GalCer tetramer⁻ NKT cells. In freshly isolated splenic MNCs, NK1.1⁻CD1d/α-GalCer tetramer$^+$ NKT cells and NK1.1$^+$CD1d/α-GalCer tetramer$^+$ NKT cells comprised CD4$^+$CD8⁻ cells (70-80%) and CD4⁻CD8⁻ (DN) cells (20-30%). α-GalCer-activated NK1.1⁻ CD1d/α-

GalCer tetramer^{+} NKT cells also consist of CD4^{+}CD8^{-} T cells (50±8%) and CD4^{-}CD8^{-} (DN) T cells (47±5%). In contrast to NK1.1^{-}CD1d/α-GalCer tetramer^{+} NKT cells, NK1.1^{+}CD1d/α-GalCer tetramer^{-} NKT cells (with or without α-GalCer) comprised CD4^{-}CD8^{+} cells and DN cells. Approximately half of the α-GalCer-activated CD8^{+}NK1.1^{+} cells were CD8 αα homodimers. NK1.1^{+}CD1d/α-GalCer tetramer^{+} NKT cells expanded with IL-2 and α-GalCer consisted of CD4^{+} cells, DN cells and approximately 10% CD8^{+} cells.

3.2 Cytokine production by three subsets of *ex vivo* α-GalCer activated-NKT cells: Several investigators have reported that NKT cells secrete large amounts of cytokines after α-GalCer or TCR/CD3 stimulation, particularly IFN-γ and IL-4. We therefore examined whether α-GalCer activated-NKT cells produce these cytokines. After culture with IL-2 and α-GalCer or IL-2 alone, supernatants were harvested on days 4, 6 and 8 and analyzed for IFN-γ and IL-4 production by ELISA. Splenic MNCs cultured with IL-2 and α-GalCer produced large amounts of IL-4 (16.9±2.2 ng/ml) and IFN-γ (22.0±3.4 ng/ml) from day 4 to day 6. However, these cytokines could not be detected in supernatant from cells cultured with IL-2 alone.

Next, we examined which NKT cell subsets produce IFN-γ or IL-4. On day 6, cultured cells were collected and stained with intracellular IFN-γ or IL-4. Remarkably, a clear difference in cytokines produced by NK1.1[-]CD1d/α-GalCer tetramer^{+} NKT cells, NK1.1[+]CD1d/α-GalCer tetramer^{-} NKT cells and NK1.1[+]CD1d/α-GalCer tetramer[+] subsets were observed. NK1.1[-]CD1d/α-GalCer tetramer^{+} NKT cells produced IFN-γ and IL-4, whereas NK1.1[+]CD1d/α-GalCer tetramer^{-} NKT cells and NK1.1[+]CD1d/α-GalCer tetramer^{+} NKT cells only produced IFN-γ. In contrast to α-GalCer-activated NKT cells, intracellular cytokines could not be detected with cells cultured using IL-2 alone. In NK1.1^{-}CD1d/α-GalCer tetramer^{+} NKT cells, both CD4^{+} and DN T cells produced IFN-γ and/or IL-4. In NK1.1^{+}CD1d/α-GalCer tetramer^{-} NKT cells, both CD8^{+} cells and DN T cells produced IFN-γ.

4. Expansion of α-GalCer-Stimulated human Vα24^{+} NKT Cells under non-FBS Culture Conditions

Efficient expansion of Vα24^{+} NKT (Vα24^{+} CD3^{+}) cells from granulocyte colony-stimulating factor (G-CSF)-mobilized peripheral blood (PB) cells is possible under culture conditions with α-GalCer, IL-2 and fetal bovine serum (FBS) *in vitro*[6]. In an attempt to avoid potential risks associated with FBS and to establish a clinical-scale expansion system, we investigated the development of a more efficient non-FBS expansion system for Vα24^{+} NKT cells with α-GalCer and IL-2.

4.1 Efficient expansion of Vα24$^+$ NKT cells in autologous plasma: In order to investigate a suitable non-FBS medium for Vα24$^+$ NKT cell expansion, PB mononuclear cells (PBMCs) obtained from PB of normal healthy volunteers were cultured in medium containing α-GalCer, IL-2 and conditioned medium comprising: 10% FBS; 10% recombinant human serum albumin (rHSA); and 10% or 5% autologous plasma or 10% or 5% autologous serum. Vα24$^+$ NKT cells were unable to proliferate in medium containing rHSA. Medium containing 5% autologous plasma promoted optimal growth of Vα24$^+$ NKT cells both in the presence of α-GalCer and IL-2. No significant differences were observed between Vα24$^+$ cell expansion in 10% or 5% autologous plasma or serum.

4.2 G-CSF mobilization augmented Vα24$^+$ NKT cell expansion: Next, we studied culture efficiency for PBMCs and medium containing 5% autologous plasma derived from G-CSF-mobilized donors. Expansion ratios of Vα24$^+$ NKT cells in a combined culture of PBMC and plasma before and after G-CSF mobilization were approximately 350-fold (before) and 2000-fold (after), respectively. Both PBMCs and plasma obtained from PB of normal healthy donors after G-CSF mobilization displayed maximal conditions for expansion of Vα24$^+$ NKT cells. Although the percentage of Vα24$^+$ NKT cells in G-CSF-mobilized PB was dramatically decreased compared to that from non-mobilized donors, Vα24$^+$ NKT cells after G-CSF mobilization expanded more efficiently than before G-CSF mobilization. These results suggest that selective expansion of Vα24$^+$ NKT cells is induced by administration of G-CSF.

4.3 Both G-CSF-mobilized PBMC and associated plasma affect Vα24$^+$ NKT cell expansion: To determine which components affect cell expansion after G-CSF mobilization, several cross-combinations of pre- and post-G-CSF conditioned PBMCs and plasma were used. Optimal combination was obtained when post-G-CSF conditioned PBMCs and post-G-CSF conditioned plasma were combined. These results suggest that the G-CSF mobilization procedure conferred a proliferating advantage to Vα24$^+$ NKT cells upon both PBMCs and associated plasma.

4.4 G-CSF induced changes in cytokine concentration in PB: Analysis of plasma before and after G-CSF mobilization revealed that levels of serum cytokines such as G-CSF, IL-3, IL-7 and IL-13 were increased after mobilization.

4.5 Kinetics of expanded cell populations with IL-2 and α-GalCer: Cell subsets in an expansion of Vα24$^+$ NKT cells were monitored on days 0, 7, 14 of culture using apheresis of PBMCs in the presence of autologous plasma. Of note is the fact that on day 0, the percentage of Vα24$^+$ NKT cells was extremely low (0.10%). The percentage of monocytes was approximately 30%, which was markedly higher than that observed before G-CSF administration (2.7-7.9%). The CD4/CD8 T cell ratio was >1. Vα24$^+$ NKT cells under

stimulation with α-GalCer displayed linear propagation until day 14. CD8 T cells (but not CD4 T cells) also expanded, becoming the predominant population. The CD4/CD8 T cell ratio was thus reversed to <1. Both B cells and monocytes completely disappeared by day 14 (2.33% and 0.16%, respectively). Given the results of our previous study, the abnormally extended percentage of monocytes on day 0 might contribute to an efficient expansion of V$_α$24$^+$ NKT cells.

4.6 **Intracellular cytokine production and cytotoxic activity of V$_α$24$^+$ NKT cells:** We purified expanded V$_α$24$^+$ NKT cells after 14 days of culture and assessed both intracellular cytokine production and cytotoxic activity of these cells. The percentage of IFN-γ-producing cells among purified V$_α$24$^+$ NKT cells was 75%, while that of IL-4-producing cells was 16%. Using PBMCs after G-CSF mobilization, V$_α$24$^+$ NKT cells predominantly produced IFN-γ instead of IL-4. Cytotoxic assay was measured against several cell lines, including Daudi, K562, Jurkat, HCT-15, HT-29, WiDr, SKOV3, and OVCAR-3 lines. Expression of CD1d molecules on target tumor cells was evaluated using CD1d mAb. Some of these target cells (Daudi and Jurkat) expressed CD1d molecule, while others did not. Purified V$_α$24$^+$ NKT cells displayed powerful cytotoxicity against all target tumor cell lines, particularly the hematological cell lines. This cytotoxicity was not related to expression of CD1d molecules on target cells. Expanded V$_α$24$^+$ NKT cells in a combined culture of PBMCs and plasma obtained from apheresis after G-CSF mobilization retained their surface markers and production of IFN-γ and IL-4, and exerted powerful cytotoxic effects against tumor cells in a CD1d-independent manner. In conclusion, the results presented herein suggest that a new expansion strategy for V$_α$24$^+$ NKT cells under non-FBS culture conditions using α-GalCer and IL-2 with G-CSF-mobilized PBMC and plasma offers the possibility of NKT immune cell therapy for cancer patients.

References

1. Kawano T, Cui J, Koezuka Y, Toura I, Kaneko Y, Motoki K, Ueno H, Nakagawa R, Sato H, Kondo E, Koseki H, and Taniguchi M. CD1d-restricted and TCR-mediated activation of valpha14 NKT cells by glycosylceramides. Science. 278, pp.1626-1629, 1997.

2. Maruoka H, Ikarashi Y, Shinohara K, Miyata M, Sugimura T, Terada M, and Wakasugi H. A novel monoclonal antibody permitting recognition of NKT cells in various mouse strains. BBRC, 242: pp.413-418, 1998.

3. Shinohara K, Ikarashi K, Maruoka H, Miyata M, Sugimura T, Terada M, and Wakasugi H. Functional and phenotypical characteristics of hepatic NK-like T cells in NK1.1-positive and -negative mouse strains. Eur. J. Immunol., 29: pp.1871-1878, 1999.

4. Azuma M, Kato K, Ikarashi Y, Asada-Mikami R, Maruoka H, Takaue Y, Saito A, Wakasugi H. Cytokines production of U5A2-13-positive T cells by stimulation with glycolipid α-galactosylceramide. Eur. J. Immunol., 30:.pp.2138-2146, 2000.

5. Kato K, Ikarashi Y, Sugahara T, Yasumoto A, Sancho D, Yoshida M, Takaue Y, Kobayashi Y, Sanchez-Madrid F, and Wakasugi H. U5A2-13, an antigen originally found on mouse NK-like T Cells, is an early inducible cell surface antigen during lymphoid activation. Cellular Immunology, 221: pp.27-36, 2003.

6. Asada-Mikami R, Heike Y, Harada Y, Kanai S, Ikarashi Y, Kato K, Shirakawa K, Takaue Y, Abe T, and Wakasugi H. Increased expansion of Valpha24$^+$ T cells derived from G-CSF-mobilized peripheral blood stem cells as compared to peripheral blood mono-nuclear cells following alpha-galactosylceramide stimulation. Cancer Science. 94, pp. 383-388, 2003.

Dr. Hiro Wakasugi, M.D., Ph.D.

1971-1982	Surgeon, Department of Surgery, Jichi Medical School
1982-1992	Directeur de Recherche of INSERM at URA 1156 CNRS, Institut Gustave-Roussy, France
1992-1993	Visiting Research Fellow, Genetics Division, National Cancer Center Research Institute
1993-1998	Chief, Section for Studies of Host-Immune Response, National Cancer Center Research Institute
1998-	Chief, Pharmacology Division, National Cancer Center Research Institute

Specialty and Present Interest:

Tumor Immunology, Cancer Immunotherapy

Clinical Data

Clinicopathological statistics on registered prostate cancer patients in Japan: 2000 report from the Japanese Urological Association

CANCER REGISTRATION COMMITTEE OF THE JAPANESE
UROLOGICAL ASSOCIATION

Abstract   *Background*: The purpose of the present paper was to investigate etiology, diagnosis, initial treatment, pathological findings and final outcomes for prostate cancer in Japan.
Methods: From 2001, the Japanese Urological Association initiated computer-based registration of prostate cancer patients in Japan to estimate etiology, diagnosis, initial planed treatment, pathological findings and final outcome.
Results: A total of 173 institutions responded and 4529 patients who were diagnosed with prostate cancer in 2000 were registered. In the first year, background factors, diagnostic procedures and initially planned treatment were recorded. The analysis of these registered cases is presented here. Nearly 30% of the cases demonstrated <10 ng/mL of prostate specific antigen. The six-core biopsy was the most commonly used procedure. The clinical T staging distribution was as follows: T1c, 20.3%; T2a, 21.8%; T2b, 17.3%; T3a, 15.8%; T3b, 11.0%; and T4, 8%. More than 70% of cases were diagnosed as M0. Hormone therapy alone was the initial treatment plan in more than half of the cases.
Conclusion: This is the first report on prostate cancer patients in Japan based on multi-institutional registration. Pathological findings and final outcome will be surveyed later by the Japanese Urological Association. After 5 years, adopted treatment, pathological results and final outcome will be registered.

Key words   epidemiology, Japan, neoplasm, prostate.

Introduction

Prostate cancer is known around the world as a disease of elderly men. Parkin *et al.* reported that three-quarters of cases occur in men over 65 years of age.[1] In Japan, although the incidence of prostate cancer has been much less than in American and European countries, it has been sharply rising during the last two decades, a trend also observed in other Asian countries. Even before the introduction of prostate specific antigen (PSA) testing in the early 1990s, incidence rates had been rising in

Correspondence: Hiroyuki Fujimoto MD, Urology Division, National Cancer Center Hospital, 5-1-1 Tsukiji, Chuo-ku, Tokyo 104-0045, Japan.
Email: juacr@nifty.com, juacr@ml.res.ncc.go.jp

many countries.[1–5] Changes from traditional Japanese to more Western lifestyles and nutritional habits have been implicated in the increase in the incidence of prostate cancer in Japan.[3] In the early 1990s, the PSA test contributed to the earlier diagnosis of prostate cancer, which is also reflected in the increased incidence. Now, in Japan as in other developed countries, prostate cancer is a large and growing public health problem whose risk factors are essentially unknown.

The precise nature of this problem differs from one country to another because of the wide range of national incidence and, to a much lesser degree, survival profiles that have been reported.[1,5–8] Recently, however, Nakata *et al.*[4] reported that the mortality rate of prostate cancer patients in Japan has been increasing as rapidly as the incidence, while in North America the mortality rate has actually declined even in the face of rising incidence.[9]

The Japanese Urological Association (JUA) and the Japanese Society of Pathology revised the 2nd edition of *General Rule for Clinical and Pathological Studies on Prostate Cancer* to the 3rd edition in 2001[10] and, in accordance with this new edition, initiated a study to estimate the etiology, diagnosis, initial treatment, pathological findings and final outcomes for prostate cancer in Japan by employing computer-based registration of prostate cancer patients from institutions all over Japan. The registration program has been established by the members of committee for revision of *General Rule for Clinical and Pathological Studies on Prostate Cancer*. Here we report the background data at diagnosis from the initial registration of 4529 patients who were diagnosed pathologically with prostate cancer in 2000.

Methods

Using a CD-ROM program developed by the members of committee for revision of *General Rule for Clinical and Pathological Studies on Prostate Cancer* and the staff of the National Cancer Center, new patients who were diagnosed by pathology to have prostate cancer in 2000 were registered. Age, occupation, race, concomitant malignancy, family history, past history and symptoms were entered as background factors for each prostate cancer patient. The findings from digital rectal examination (DRE), imaging, PSA level, number of cores taken by biopsy, number of positive core(s), histology of the biopsy specimen, Gleason score, 5th tumor, nodes, metastases (TNM) classification (5th edition), diagnostic process and initial treatment plan were also entered. The collected data were analyzed.

Results

One hundred and seventy-three institutions responded and 4529 patients who were diagnosed with prostate cancer in 2000 were registered. Approximately 14 000 new prostate cancer patients were estimated in Japan this year;[9] therefore, approximately 30% of total cases were covered by this registry.

Background data

The age distribution of patients is summarized in Figure 1. More than one-quarter of all patients were 70–74 years old, and three-quarters were 60–79 years old. The ethnic distribution was as follows: Japanese, 99.56%; non-Japanese Mongolians, 0.29%; and Caucasian, 0.13%. Only 71 patients (1.57%) had a family
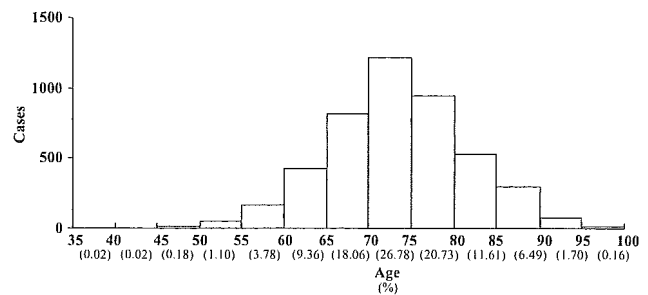

Fig. 1 Age distribution of prostate cancer newly diagnosed in 2000 and registered. Registered cases were divided into 5-year age groups as indicated. Bars indicate the number of cases equal to and above the age on the left lower corner and below the age on the right lower corner of each bar. The numbers below each bar indicate the percentage of cases in each age group among all registered cases.

Table 1 Findings of local imaging study

	n	(%)
Not visible	1255	27.71
Confirmed within prostate	1580	34.89
Extra-capsule	732	16.16
Invades adjacent structure	685	15.12
Uncertain	277	6.12
Total	4529	100.00

history of prostate cancer in either their father (0.66%), brother (0.82%), or uncle (0.09%). Common occupations of the registered patients were the following: retired (61.29%), office clerks or associate professionals (8.06%), corporate or general managers (6.93%), agricultural, forestry, or fishery workers (6.71%), and professionals or technicians (6.62%). A total of 520 patients (11.48%) had a history of other malignancies.

Initial evaluation

Of all the patients, 71.08% (3219 cases) presented with some symptoms and 339 cases (7.49% of all and 35.17% of metastatic disease) presented with symptoms from metastases.

The most commonly used staging modalities were transrectal ultrasonography (TRUS; 78.32%) and bone scan (73.53%), followed by computed tomography (CT; 66.75%) and magnetic resonance imaging (MRI; 42.77%). The findings from local imaging studies are summarized in Table 1. As expected, local imaging studies yielded better sensitivity (66.17% produced a positive finding) than DRE (58.29% true-positives; Table 2).

Table 2 Findings of digital rectal examination

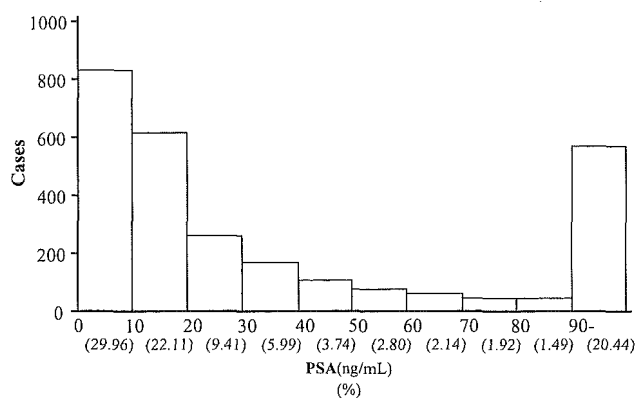|	*n*	(%)
Not palpable	1706	37.67
One lobe	1090	24.07
Both lobe	760	16.78
Extra-capsule	481	10.62
Seminal vesicle invasion	113	2.50
Extra-prostate	196	4.33
Uncertain	18.3	4.04
Total	4529	100.00

Fig. 2 Distribution of prostate specific antigen (PSA) value of registered cases. Registered cases were divided into groups of PSA value by 10 ng/mL as indicated. The PSA value was measured by Tandem-R and includes all Tandem-R compatible kits, such as *E*-test Tosoh, Chemi-lumi ACS-PSA, Shifalite PSA and Lumipulse PSA. Bars indicate the number of cases equal to and above the value on the left lower corner and below the value on the right lower corner of each bar. Cases with PSA ≥ 90 ng/mL were counted as a single group. The numbers below each bar indicate the percentage of cases in each group among all registered cases.

Table 3 Number of adopted biopsy cores

Core(s)	*n*	(%)
1	5	0.12
2	93	2.30
3	52	1.28
4	264	6.52
5	90	2.22
6	2128	52.52
7	282	6.96
8	616	15.20
9	90	2.22
≥10	432	10.66
Total	4052	100

Uncertain, 168 patients.

Table 4 Primary Gleason grade

Gleason grade	*n*	(%)
1	376	8.30
2	541	11.90
3	1155	25.50
4	695	15.30
5	308	6.80
Uncertain	1454	32.10
Total	4529	100

Table 5 Secondary Gleason grade

Gleason grade	*n*	(%)
1	251	5.50
2	552	12.20
3	1020	22.50
4	780	17.20
5	312	6.90
Uncertain	1614	35.60
Total	4529	100

The PSA level distribution is summarized in Figure 2. Nearly 30% of prostate cancer cases diagnosed in 2000 demonstrated a PSA value of <10 ng/mL.

A summary of the biopsy statistics is shown in Tables 3–5 and Figure 3. Because the same number of cores is usually taken from each lobe, the 5th, 7th, and 9th core samples are supposed to be additional targeted biopsies of suspicious lesions (Table 3). The percentage of biopsies yielding all positive cores was higher for the 6-core than for the 8-core biopsy (Fig. 3). However, the percentage of biopsies yielding only one positive core was higher for the 8-core procedure. A total of 99.8% of tumors were determined pathologically to be adenocarcinoma, followed by neuroendocrine tumors (0.1%). Moderately differentiated adenocarcinoma (43.5%) was

the most common differentiation state found in this population, followed by well-differentiated (31.3%) and poorly differentiated adenocarcinomas (20.6%). Gleason grade classification is summarized in Tables 4,5; grade 3 was found to be the most common grade in both primary and secondary dominant tumors.

Initial staging

Clinical T stage of this population is summarized in Figure 4. The clinical T staging distribution is as follows: T1c, 20.3%; T2a, 21.8%; T2b, 17.3%; T3a, 15.8%; T3b, 11.0%; and T4, 8%. Regionally limited lymph node metastases examined mainly by CT were found in 501 cases (11.06%), and 3569 cases
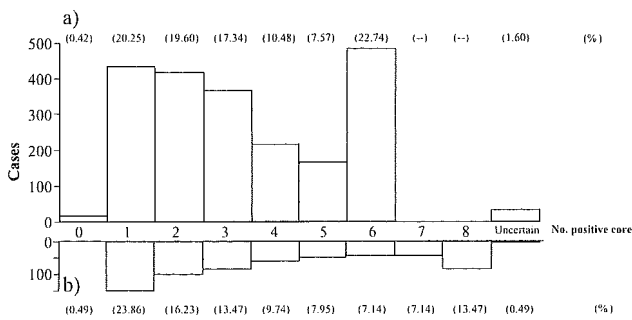
a)

(0.42) (20.25) (19.60) (17.34) (10.48) (7.57) (22.74) (--) (--) (1.60) (%)

No. positive core

(0.49) (23.86) (16.23) (13.47) (9.74) (7.95) (7.14) (7.14) (13.47) (0.49) (%)

Fig. 3 Number of cancer-positive cores in (a) 6-core biopsy ($n = 2128$) and (b) 8-core biopsy ($n = 616$). Registered cases were divided into groups by number of cancer-positive cores as indicated. Bars indicate the number of cases in each group. The percentage of cases in each group among each subgroup of 6- or 8-core biopsy is indicated over or below the bars.
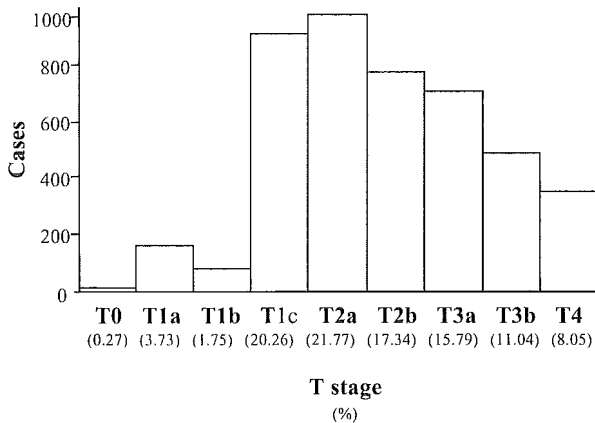

T0   T1a   T1b   T1c   T2a   T2b   T3a   T3b   T4
(0.27) (3.73) (1.75) (20.26) (21.77) (17.34) (15.79) (11.04) (8.05)

T stage
(%)

Fig. 4 Distribution of local staging (T staging). Registered cases were divided into groups by local staging as indicated according to the 1997 International Union Against Cancer (UICC) tumor, nodes, metastases (TNM) classification. Bars indicate the number of patients for each T stage. The numbers below each bar indicate the percentage of cases in each age group among all registered cases.

(78.80%) were diagnosed as negative lymph node metastasis.

Distant metastases are detailed in Table 6. More than 70% of patients were negative for distant metatstasis.

Initial treatment strategies

Selected plans are summarized in Figure 5. Hormonal therapy alone was chosen for more than half of the cases. Prostatectomy with or without hormonal therapy was planned for 27.4% (1240 cases). Irradiation with or without hormonal therapy was not very common (8.1%). For cases of T1c to T3N0M0 (2671 cases total),

Table 6 M stage

M stage	n	(%)
M0	3243	71.61
M1a	40	0.88
M1b	861	19.01
M1c	63	1.39
MX	322	7.11
Total	4529	100

a)   Treatment   b)
Cases 2000   1000   0   0   1000 Cases

(5.59)   W/W   (2.92)
(13.43)   RRP   (19.73)
(13.96)   Hx+RRP   (19.02)
(0.71)   Hx+RRP+Rx   (0.97)
(2.05)   Rx   (3.22)
(6.01)   Hx+Rx   (7.60)
(56.94)   Hx   (45.90)
(0.37)   Others   (0.30)
(0.95)   Uncertain   (0.00)
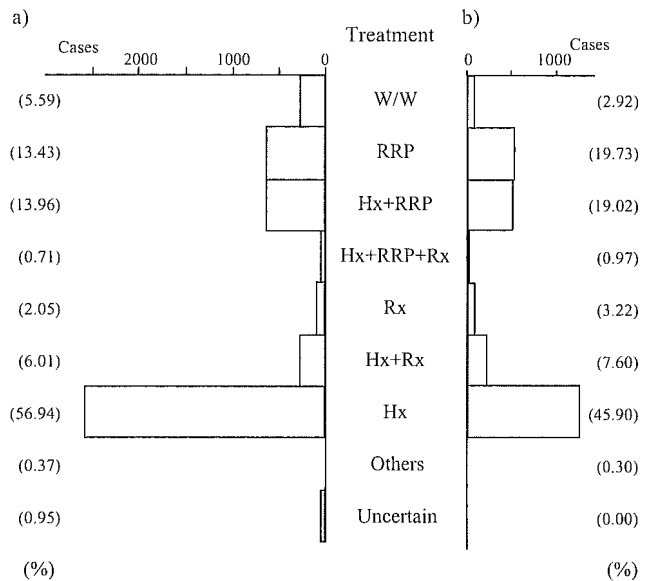(%)   (%)

Fig. 5 Initial treatment plan for (a) all registered cases ($n = 4529$) and (b) cases of T1c to T3 without lymph node or distant metastases ($n = 2671$). Registered cases were divided into groups by initial treatment plan, which includes each treatment modality and appropriate combinations, as indicated. W/W, watchful waiting; RRP, retropubic radical prostatectomy; Hx, hormonal therapy; Rx, irradiation. Bars indicate the number of cases in each group. The numbers below each bar indicate the percentage of cases in each group among all registered cases or the subgroup of patient at stage T1c to T3 without lymph node or distant metastases.

45.90% (1226 cases) were scheduled to undergo hormonal therapy without any other additional treatment. Irradiation was not commonly advised for this group (10.8%).

Additional data are summarized in Appendix I–IV.

Acknowledgments

Urology, National Cancer Center, Tokyo), and Ms M Nakamura, a secretary of cancer registration office, for special efforts to analyze and summarize the data.

This document was established by the Cancer Registration Committee of the Japanese Urological Association. Members of this task force include: Hiroyuki Fujimoto, MD, National Cancer Center Hospital, Tokyo; Tsuneharu Miki, MD, Chair, Cancer Registration Committee of the Japanese Urological Association, Kyoto University of Medicine, Kyoto; Masaru Murai, MD, Keio University School of Medicine, Tokyo; Tomoaki Fujioka, MD, Iwate Medical Univeristy School of Medicine, Iwate; Seiji Naitoh, MD, Graduate School of Medical Science, Kyushu University, Kyushu; Tadao Kakizoe, MD, National Cancer Center, Tokyo; Akihiko Okuyama, MD, Graduate School of Medical Science, Kyushu University, Kyushu; Hideyuki Akaza, MD, Institute of Clinical Medicine, University of Tsukuba, Tsukuba; Youichi Mizutani, MD, Kyoto University of Medicine, Kyoto; and Sadao Kamidono, MD, Kobe University School of Medicine, Kobe, Japan.

Member of the Cancer Registration Committee of Japanese Urological Association

This document was established by the Cancer Registration Committee of Japanese Urological Association. Members of this task force include: Hiroyuki Fujimoto, MD, National Cancer Center hospital, Tokyo; Tsuneharu Miki, MD, Chair, Cancer Registration Committee of Japanese Urological Association, Kyoto University of Medicine, Kyoto; Masaru Murai, MD, Keio University School of Medicine, Tokyo; Tomoaki Fujioka, MD, Iwate Medical University School of Medicine, Iwate; Seiji Naito, MD, Graduate School of Medical Science, Kyushu University, Kyushu; Tadao Kakizoe, MD, National Cancer Center, Tokyo; Akihiko Okuyama,

MD, Graduate School of Medicine, Osaka University, Osaka; Hideyuki Akaza, MD, Institute of Clinical Medicine University of Tsukuba, Tsukuba; Youichi Mizutani, MD, Kyoto University of Medicine, Kyoto; Sadao Kamidono, MD, Kobe University School of Medicine, Kobe.

References

1   Parkin DM, Bray FI, Devesa SS. Cancer burden in the year 2000. *Eur. J. Cancer* 2001; **37** (Suppl. 8): 4–66.
2   Breslow N, Chan CW, Dhom G *et al.* Latent carcinoma of prostate at autopsy in seven areas. *Int. J. Cancer* 1977; **20**: 680–8.
3   Akazaki K, Stemmermann GN. Compararative study of latent carcinoma of the prostate among Japanese in Japan and Hawaii. *J. Natl Cancer Inst.* 1973; **50**: 1137–44.
4   Nakata S, Takahashi H, Ohtake N, Takei T, Yamanaka H. Trends and characteristics in prostate cancer mortality in Japan. *Int. J. Urol.* 2000; **7**: 254–7.
5   Quinn M, Babb P. Patterns and trends in prostate cancer incidence, survival, prevalence and mortality. Part I. International comparisons. *BJU Int.* 2002; **90**: 162–73.
6   Parkin DM, Pisani P, Ferlay J. Estimates of the world-wide incidence of 25 major cancers in 1990. *Int. J. Cancer* 1999; **80**: 827–41.
7   Coleman MP, Esteve J, Damieki P *et al. Trends in Cancer Incidence and Mortality.* IARC. Scientific Publications no. 121. International Agency for Research on Cancer, Lyons, 1993.
8   Whittlemore AS. *Trends in Cancer Incidence and Mortality. Cancer Surveys, Vol. 19, 20.* Imperial Cancer Research Fund/Cold Spring Harbor Laboratory Press, New York, 1994.
9   The Research Group for Population-based Cancer Registration in Japan. Cancer incidence and incidence rates in Japan in 1997: estimates based on data from 12 population-based cancer registries. *Jpn J. Clin. Oncol.* 2002; **32**: 318–22.
10 Japanese Urological Association and The Japanese Society of Pathology. *General Rule for Clinical and Pathological Studies on Prostate Cacner.* Kanehara, Tokyo, 2001.

Appendix
I. General statistics

I.1. Background

I.1.1. Races

Race	Number	%
Japanese	4509	99.56
Mongolian (without Japanese)	13	0.29
White	6	0.13
Uncertain	1	0.02
Total	4529	100

I.1.3. Occupation

Occupation	Number	%
Service workers	101	2.23
Transportal and postal related workers	63	1.39
Corporate and general managers	314	6.93
Craft, related trades workers and elementary occupations	165	3.64
Mining labourers	8	0.18
Office clerks and associate professionals	365	8.06
Professionals and technicians	300	6.62
Agricultural, forestry and fishery workers	304	6.71
Sales workers	119	2.63
Protective services workers	14	0.31
Others or retired	1002	22.12
Uncertain	1774	39.17
Total	4529	100

I.1.2. Family history of prostate cancer

	Number	%
Father	30	0.66
Brother	37	0.82
Uncle	4	0.09
Total	71	1.57

I.1.4. Distribution of organs of concomitant malignancy

Organ	Number
Kidney	33
Urothelial	111
Testis	2
Penile	3
Head and neck	34
Lung	50
Esophageal	10
Stomach	107
Colon	120
Liver and gall bladder	19
Pancreas	9
Skin	6
Hematological	8
Sarcoma	3
Breast	1
Uncertain and other	4
Total	520
Negative	4022

I.2. Symptoms

I.2.1. Urological

Symptoms	Number	%
+	3219	71.08
–	1273	28.11
Uncertain	37	0.82
Total	4529	100

I.2.2. Metastatic

Symptoms	Number	%
+	339	7.49
–	4137	91.34
Uncertain	53	1.17
Total	4529	100

I.3. Staging method and findings

I.3.1. Modality of image study

Number		% in all cases
CT	3023	66.75
MRI	1937	42.77
Bone scan	3330	73.53
TRUS	3547	78.32